3-D α colony characterisation and prior-β grain reconstruction of a lamellar Ti-6Al-4V specimen using near-field high energy x-ray diffraction microscopy

E. Wielewski[a,c,d], D. B. Menasche[a], P. G. Callahan[b,e] and R. Suter[a]

[a] Department of Physics, Carnegie Mellon University, Pittsburgh, PA 15213, USA

[b] Department of Materials Science and Engineering, Carnegie Mellon University, Pittsburgh, PA 15213, USA

[c] Sibley School of Mechanical and Aerospace Engineering, Cornell University, Ithaca, NY 14853, USA

[d] School of Engineering, University of Glasgow, Glasgow, G12 8QQ, UK

[e] Materials Department, University of California at Santa Barbara, Santa Barbara, CA 93106, USA

Correspondence email: Euan.Wielewski@glasgow.ac.uk

Abstract

Near-field high energy X-ray diffraction microscopy (nf-HEDM) has been used to characterize the 3-D crystallographic orientation field of the hexagonal close-packed (hcp) α phase in a bulk Ti-6Al-4V specimen with a lamellar (β-annealed) microstructure. These data have been segmented using a 3-D misorientation-based grain finding algorithm, providing unprecedented information about the complex 3-D morphologies and spatial misorientation distributions of the transformed α lamellae colonies. A 3-D Burgers orientation relationship-based flood fill algorithm has been implemented to reconstruct the morphologies and crystallographic orientations of the high temperature body centred cubic (bcc) prior-β grains. The combination of these data has been used to gain understanding of the role of the prior-β grain structure on the formation of specific morphologies and spatial misorientation distributions observed in the transformed α colony structures. It is hoped that this understanding can be used to develop transformation structures optimized for specific applications and to produce more physically realistic synthetic microstructures for use in simulations.

1. Introduction

The industrially important dual-phase titanium alloy, Ti-6Al-4V, can be processed to have a number of different microstructural forms. When processed through the thermo-mechanical route outlined in Figure 1, the so-called lamellar (or β-annealed) microstructural form is obtained, consisting of colonies of lamellae of the room-temperature hexagonal close-packed (hcp) α phase in a matrix of the retained high-temperature body-centred cubic (bcc) β phase (Lutering & Williams, 2003). The solid state β to α phase transformation is known to yield complex α phase geometries that are sensitive to details of the thermo-mechanical processing.
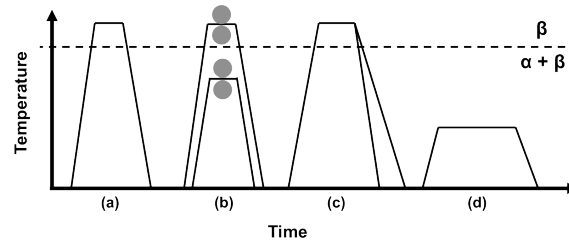
Figure 1: Thermo-mechanical processing route for lamellar (β-annealed) Ti-6Al-4V, consisting of (a) homogenisation, (b) deformation, (c) recrystallisation and (d) annealing.

The crystallographic orientations of the transformed α lamellae colonies are related to the orientation of their high-temperature parent β grain through the well-established Burger's orientation relationship (BOR) (Burgers, 1934):

$$\{110\}_\beta \parallel (0002)_\alpha$$
$$[111]_\beta \parallel [11\bar{2}0]_\alpha$$

Due to its extensive use within the aerospace industry, the mechanical behaviour of Ti-6Al-4V is of particular interest to materials scientists and engineers. Key microstructural parameters that have been shown to determine the mechanical properties of lamellar Ti-6Al-4V include: α lamellae width, α lamellae colony size/morphology, prior-β grain size/morphology and crystallographic texture (Lutering & Williams, 2003).

Recent advances in near-field high-energy X-ray diffraction microscopy (nf-HEDM) at the Advanced Photon Source (APS) (Lienert et al., 2011), combined with the forward modeling

method (FMM) for crystallographic orientation reconstruction (Suter et al., 2006; Li & Suter, 2013), have made it possible to nondestructively reconstruct spatial maps of local crystal orientations in 3-D with unprecedented detail. Current nf-HEDM experimental procedures at the APS have been shown to give spatial resolutions of ~1 µm, with orientation resolutions of ~0.1° (Lienert et al., 2011; Li & Suter, 2013). In the FMM for orientation reconstruction, the interrogated volume of material is virtually discretized into space-filling voxels, with the orientation of each voxel optimized by comparison between simulated and experimental diffraction peaks for multiple detector distances. The FMM has been successfully applied to a growing number of materials and conditions, such as grain growth in aluminum (Hefferan et al., 2012), plastic deformation in copper (Li et al., 2012; Pokharel et al., 2015) and deformation twinning in zirconium (Lind et al., 2014).

In this paper, nf-HEDM and the FMM have been used to spatially map the local crystal orientations of α colonies in a Ti-6Al-4V specimen in 3-D. These data provide unique information on the 3-D morphology of the α colonies, as well as the misorientations developed during transformation. A flood fill based technique has also been developed to reconstruct the prior-β grains in 3-D, allowing the complex 3-D morphologies and spatial misorientation distributions of the α colonies to be directly linked to the prior-β grain structure.

2. Experiment and FMM Reconstruction

The specimen was machined from a plate of lamellar (β-annealed) Ti-6Al-4V to have a 1 x 1 mm^2 cross-section, as indicated in Figure 2, and a total length of ~8 mm. The nf-HEDM experiment was conducted at Sector 1-ID at the APS, a high brilliance and high energy X-ray beamline with dedicated nf-HEDM facilities. A schematic of the nf-HEDM experimental setup at Sector 1-ID is given in Figure 2. A 52 keV monochromatic line-focused X-ray beam, with focussed height of ~2 µm and width of ~1.2 mm, was used to interrogate x-y planar sections of the lamellar Ti-6Al-4V specimen. To study a volume of the specimen, successive layers were measured by vertically translating the specimen through the line-focussed X-ray beam in 25 µm increments. Each layer of material was interrogated by rotating the specimen through 180° around the vertical axis, denoted in Figure 2 as the z-axis, with the diffracted signal integrated over 1° increments. A scintillator and optically coupled CCD were used to record the diffracted Bragg peaks with an effective resolution of 1.48 x 1.48 µm per pixel over 2048 x 2048 pixels at rotation axis-to-detector distances of ~4.4 mm and ~6.4 mm for each layer. The orientation of

the detector relative to the laboratory reference frame and the distance of the detector relative to the rotation axis were determined by scanning a single layer of a polycrystalline gold reference specimen and conducting a detector parameter optimization. A total of 30 layers of the lamellar Ti-6Al-4V specimen were measured, corresponding to a total volume of 0.75 x 1 x 1 mm^3.
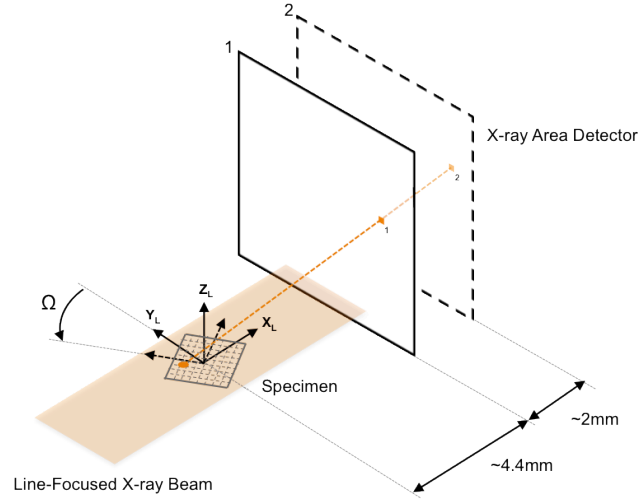
Figure 2: Schematic of nf-HEDM experimental setup.

Given the detector images for each layer, the FMM for orientation reconstruction can then be used to reconstruct the orientation field found within the specimen. The FMM for orientation reconstruction has been extensively documented elsewhere (Suter et al., 2006; Hefferan et al., 2012; Li et al., 2012; Li & Suter, 2013; Lind et al., 2014; Pokharel et al., 2015), as such, only a brief overview will be given here. For each layer, the interrogated slice of material is first discretized into 2-D triangular voxels in the plane of the line-focussed X-ray beam. The orientation of each of these voxels is then optimized by comparing simulated diffraction peaks with those observed during the experiment, using a hierarchical grid search followed by Monte Carlo-based optimization to find orientations. This results in a discrete 2-D orientation field, with each voxel having an associated orientation and confidence index that is determined by the number of overlapping simulated and experimentally observed diffraction peaks. Due to the size of the lamellae features in the Ti-6Al-4V specimen, the side length of the voxels used in the reconstruction were set at ~10 μm, while the intrinsic spatial resolution of the measurement is closer to the ~2 μm detector resolution. Data collection time was roughly 10 hours.

3. Prior-Beta Grain Reconstruction Algorithm

As a means to better understand how key microstructural features are formed during thermo-mechanical processing and to link the prior-β grain microstructure with mechanical behavior, a number of different algorithms have been developed to reconstruct the orientation and structure of the high-temperature prior-β grains based on the orientation and structure of the room-temperature α colonies.

Given the BOR and applying crystallographic symmetries, Humbert *et al.* (Humbert et al., 1995) showed that any given bcc β orientation can transform into a total of twelve different hcp α orientations, commonly referred to as variants. Likewise, any given α orientation can transform into a total of six different prior-β orientations.

Utilizing this theoretical background, Moustahfid *et al.* (Moustahfid et al., 1997a; b) were able to determine the orientation distribution function of the high-temperature bcc β phase in a Ti-6Al-4V specimen by measuring the orientations of hcp α colonies at room-temperature using electron backscatter diffraction (EBSD) and manually determining if neighboring colonies came from the same prior-β grain.

Glavicic *et al.* (Glavicic et al., 2003a; b, 2004) and Gey and Humbert (Gey & Humbert, 2003) extended this work by automating the process of reconstructing prior-β grains from large area EBSD maps of lamellar Ti-6Al-4V α colonies using voxel-to-voxel and global misorientation statistics. These and similar algorithms have been used to study a range of different processing topics, such as preferential variant selection (Bhattacharyya et al., 2003; Stanford & Bate, 2004; Sargent et al., 2012) and microstructural development during friction stir processing (Davies et al., 2011; Pilchak & Williams, 2011), with the later recently being extended to 3-D (Tiley et al., 2014).

As part of this work, a flood fill based algorithm has been developed that is capable of robustly reconstructing prior-β grain morphologies and orientations in 3-D from nf-HEDM reconstructions of the α phase in Ti-6Al-4V. Again following the theoretical background of Humbert *et al.* (Humbert et al., 1995), for any given hcp α orientation, the transformation to each of the six possible bcc β orientations can be characterized by a rotation, with each rotation being assigned a number (variant numbering). The consistently numbered bcc β orientations can then be pre-

calculated for every voxel in the nf-HEDM dataset. The voxel with the highest confidence, as determined by the FMM reconstruction, is selected as the master voxel and added to a flood fill queue. β variant "1" is then selected as the master variant. If the misorientation between the voxel from the queue (for the initial case, the master voxel) and any of the neighboring voxel's six possible β variants is less than a certain tolerance, then the neighboring voxel is added to the flood fill queue and assigned the relevant β orientation. This process is repeated until the flood fill is completed. The algorithm then returns to the master voxel and repeats the process, setting the remaining five possible β variants as master variants. The master β variant that minimizes the global misorientation, i.e. the master β variant with the largest number of voxels, is then selected as the most probable β orientation for all the flood filled voxels. The voxels that were selected by the flood fill for that β orientation are assigned a β grain number and an average β orientation is calculated using a quaternion cloud averaging method (Cho et al., 2005), before the voxels are removed from future calculations. The entire process is repeated until there are no remaining unassigned voxels in the volume. A detailed flowchart of this prior-β reconstruction algorithm is given in Figure 3.

Although computationally slower than algorithms utilizing α colony averaged orientations (Pilchak & Williams, 2011; Tiley et al., 2014), the outlined algorithm gives more robust reconstructions of the prior-β grain morphologies due to the voxel-by-voxel nature of the flood fill algorithm. This is most notably the case when considering α colonies that span two prior-β grains.

4. Results

A meshed data structure was used to analyse the nf-HEDM data, consisting of nodal points and elements defined by the nodal point connectivity. The 2-D voxels for each nf-HEDM layer were extended in the vertical direction, on either side of the 2-D layer, to give 3-D triangular prism elements with a height of 25 μm, filling the space between the nf-HEDM layers. Using the meshed data structure, neighbors are defined as elements that share element faces. This data structure allows the quick calculation of metrics between elements, such as local crystallographic misorientation. To allow further α colony and prior-β grain specific metrics to be calculated, the nf-HEDM data was segmented using a flood-fill based grain finding algorithm with a 3° misorientation criterion. The complete 3-D nf-HEDM datasets for both the α colonies and prior-β grains can be freely obtained from Wielewski et al., 2015.

A 3-D visualisation of the α colonies and prior-β grains are given in Figure 4 (a) and (b), respectively, where each colony or grain is colored by its average orientation in Rodrigues space. The average orientations of the α colonies were calculated again using the quaternion cloud averaging method (Cho et al., 2005). In the case of the α colonies, the average orientation was then used to calculate the colony (grain) relative misorientation for each voxel in the colony, allowing intra-colony spatial variations in crystallographic orientation to be easily identified.
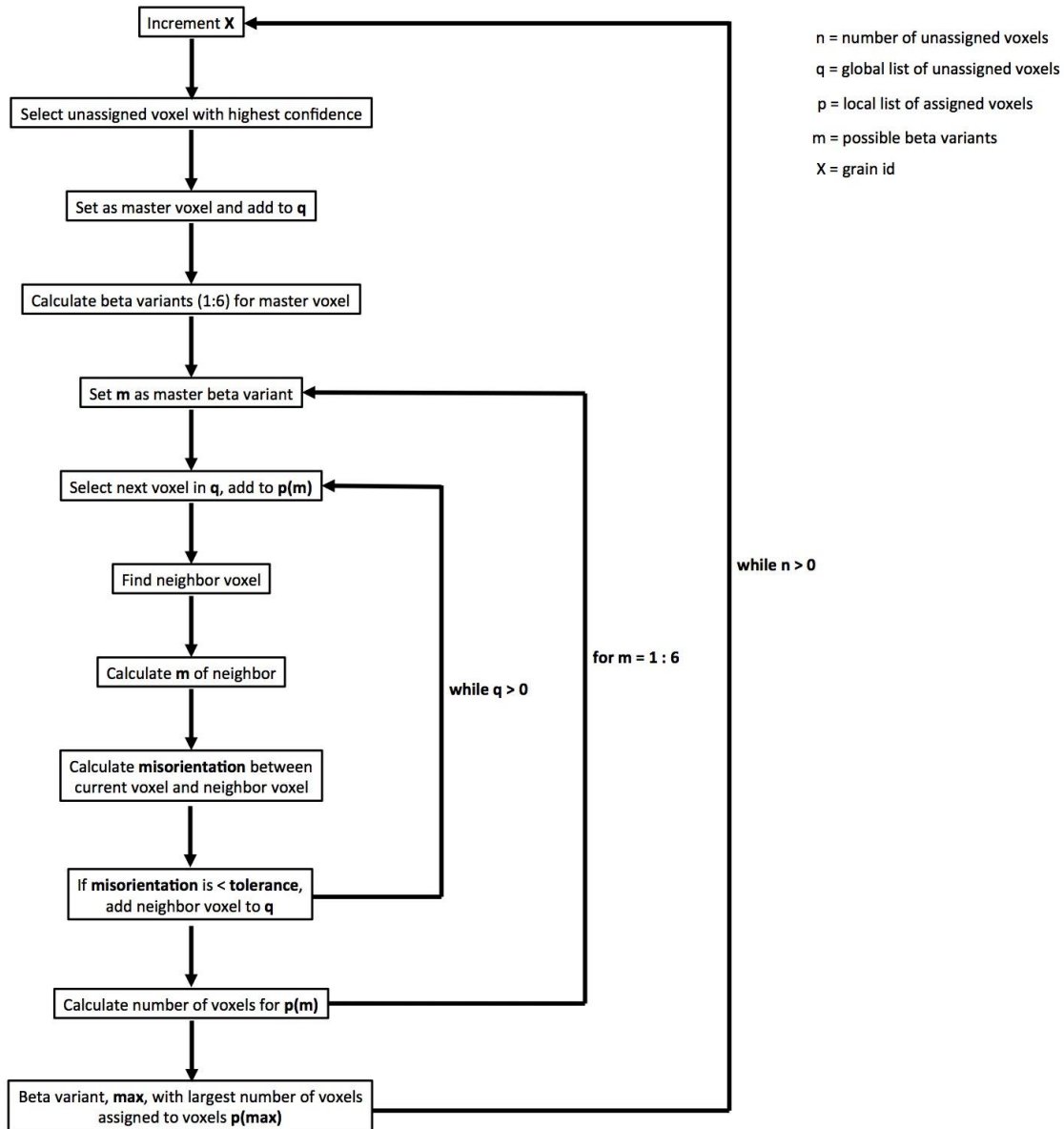

Figure 3: Prior-β grain reconstruction algorithm.
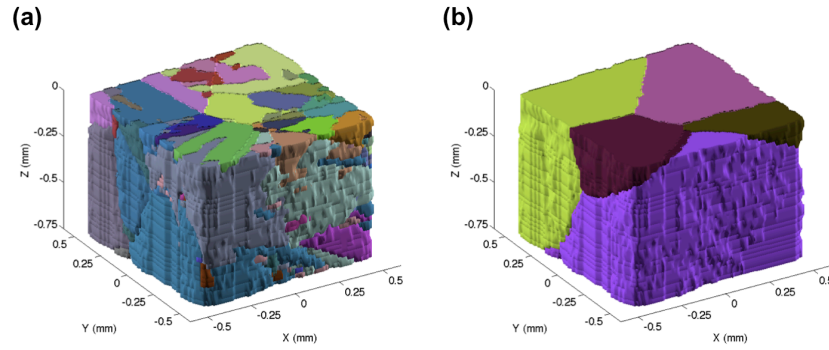
Figure 4: Full volume 3-D visualisation of data from lamellar Ti-6Al-4V specimen showing: (a) α colonies and (b) reconstructed prior-β grains. Colored by colony or grain average orientation (Rodrigues).

2-D sections of the nf-HEDM data and various calculated metrics from a single representative layer are given in Figure 5, including (a) α colonies, colored by colony average orientation with thin black lines highlighting colony boundaries and thick black lines highlighting prior-β grain boundaries, (b) prior-β grains, colored by grain average orientation with prior-β grain boundaries highlighted by thick black lines, (c) colony (grain) relative misorientation angle, with thin black lines highlighting colony boundaries and thick black lines highlighting prior-β grain boundaries and the confidence index for each voxel. The section shown is at a height of 0.375 mm, near the center of the 3-D volumes shown in Figure 4.
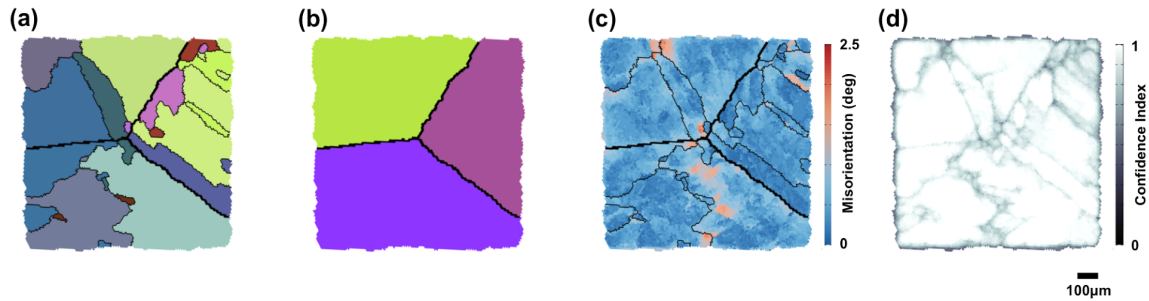
Figure 5: Example results from a single nf-HEDM layer at a height of 0.375mm showing: (a) α colonies colored by colony average orientation (Rodrigues), with colony boundaries highlighted by thin black lines and prior-β grain boundaries highlighted with thick black lines, (b) reconstructed prior-β grains colored by grain average orientation (Rodrigues), with prior-β grain boundaries highlighted by thick black lines, (c) voxel-by-voxel α colony misorientation angle (relative to colony average orientation), with colony boundaries highlighted by thin black lines and prior-β grain boundaries highlighted with thick black lines and (d) voxel-by-voxel orientation confidence index (1 = high confidence, 0 = low confidence).

3-D visualisations of individual α colonies are also given in Figure 6. The α colony shown in Figure 6(a) has a plate-like structure and was located on a prior-β grain boundary. These colonies are typically referred to as "grain boundary α". The α colony shown in Figure 6(b) is a representative example of the complex transformation structures formed in the interior of a prior-β grain. Finally, the α colony shown in Figure 6(c) is an example of an α colony that has formed at the quad node between prior-β grains, with three prior-β grain boundaries clearly visible.
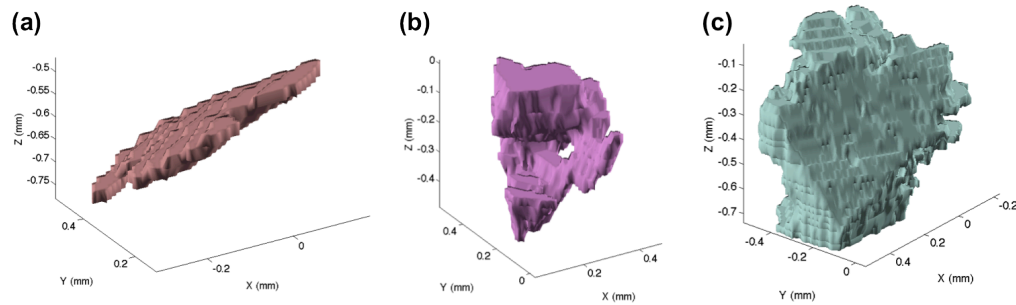
Figure 6: Example α colonies in 3-D: (a) plate-like α colony at prior-β grain boundary, (b) typical α colony with complex morphology and (c) α colony at prior-β grain quad node. Colored by colony average orientation (Rodrigues).

## 5. Discussion

4.1 α colonies and prior-β grain morphologies

As can be seen from Figure 4(b) and Figure 5(b), the reconstructed prior-β grains have a relatively equiaxed structure with well-defined grain boundaries that form flat, planar facets. Unfortunately, due to the large size and thus low number (~5) of the prior-β grains found in this microstructure, no meaningful statistics on the grain size, grain morphology or crystallographic texture could be calculated. However, the simple, polyhedral shapes of the prior-β grains do give confidence in both the nf-HEDM / FMM reconstruction and the prior-β grain reconstruction algorithm used in this work.

From Figure 4(a), Figure 5(a) and Figure 6, it can be seen that the α colonies present in the interrogated volume have a variety of morphologies, ranging from relatively simple plate-like structures to extremely complex structures that include holes, such as the α colony shown in Figure 6(b). Attempts were made to quantify the morphology of the α colonies using standard analysis techniques but, due to the wide range of complex shapes observed in the nf-HEDM

data, it was not possible to obtain meaningful results. Future work will focus on using advanced morphology analysis techniques, such as moment invariants (Callahan et al., 2013), to quantitatively describe the α colony morphologies in larger measured volumes.

4.2 α colony transformation misorientations

During transformation from the hcp α phase to the bcc β phase in Ti-6Al-4V, significant intra-colony misorientations can develop in the transformed α colonies. To better understand the relationship between an α colony's morphology, it's parent prior-β grain and the misorientation distributions developed during transformation, area normalised histograms of the intra-colony misorientation angle distributions for the α colonies shown in Figure 6 were calculated and are given in Figure 7. Intra-colony misorientations were calculated by using the colony average orientation as a reference and calculating the misorientation of each element in the colony. The colonies shown in Figure 6 and 7 were chosen as they provide representative examples of the range of α colony morphologies and misorientation distributions observed in the interrogated volume.
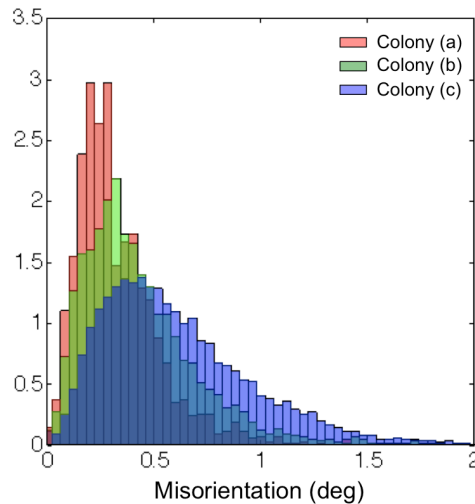
Figure 7: Area normalized histograms showing misorientation angle distributions for example α colonies given in Figure 6. Misorientations taken relative to the colony average orientation.

From the area normalised histograms shown in Figure 7, it can clearly be seen that Colony (a) has the tightest misorientation angle distribution, followed by Colony (b) and then Colony (c). As discussed in the previous section, Colony (a) has a plate-like morphology and was found at a prior-β grain boundary. This appears to allow a relatively "clean" transformation, resulting in very little misorientation development during transformation. It seems likely that this is due to the fact

that the grain boundary α colonies nucleate early in the transformation process (Lutering & Williams, 2003) and thus have very few constraints. Colony (b) is typical of α colonies that have formed in the interior of a prior-β grain. The observed morphological complexity in such colonies correlates with a wider distribution in crystallographic misorientation, as seen in Figure 7, with both likely due to interactions with other competing α colonies forming in the same prior-β grain. Finally, Colony (c) is a special case in which an α colony has formed at the quad node between prior-β grains. The constraints imposed by the prior-β grain boundaries during the transformation process appears to cause a wider misorientation distribution, as shown in Figure 7.

The role of these distributions in misorientation angle on subsequent mechanical behavior are currently being investigated and will be reported in a future article.

4.3 Single α colony spanning two prior-β grains

An additional α colony structure and its parent prior-β grains are shown in Figure 8. As can be seen, this α colony is of particular interest because it spans two prior-β grains. It has been noted that if two neighboring prior-β grains share particular misorientations then it is possible for an α variant to form that is shared between the two grains (Bhattacharyya et al., 2003). As this it is energetically preferential, it is likely that variant selection will occur and the shared α variant will be selected by both grains. The colony shown in Figure 8 highlights the robustness of the flood-fill based prior-β grain reconstruction algorithm, as a colony average based algorithm would not have been able to see the prior-β grain boundary, whereas the voxel-by-voxel nature of the flood-fill based algorithm does see the prior-β grain boundary and correctly reconstructs the prior-β grains.
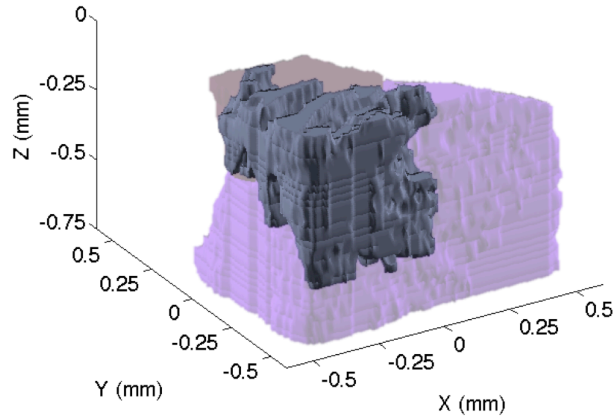
Figure 8: Single α colony spanning two prior-β grains. Colored by colony and grain average orientation (Rodrigues).

6. Conclusions

Nf-HEDM and the FMM for orientation reconstruction have been used to map the crystallographic orientations of the hcp α phase in a bulk specimen of the industrially important titanium alloy, Ti-6Al-4V. These data have been used to reconstruct the high-temperature bcc prior-β grains through the BOR and using a novel flood-fill based reconstruction algorithm. Post-processing analysis tools have also been developed to analyse nf-HEDM data in 3-D. The combination of these data and the developed analysis tools has allowed new insight into the 3-D transformation process in Ti-6Al-4V, with the orientations, morphology and intra-colony misorientation distributions of the α colonies shown to be closely linked to the orientations and morphologies of their parent prior-β grains.

Looking forward, it is expected that measurements such as these will become both increasingly detailed and more straightforward to conduct. Data collection times at the APS beamline can be expected to be reduced by as much as a factor of ten with installation of a superconducting undulator source. Larger volumes can be measured with higher spatial resolution and multiple states of a given sample can be tracked in order to understand thermal and mechanical responses. While these data sets are expensive in terms of planning, human resource requirements, and synchrotron and computational resource usage, they offer a unique means to probe materials evolution and to develop validated computational models.

References

Bhattacharyya, D., Viswanathan, G. B., Denkenberger, R., Furrer, D., & Fraser, H. L. (2003). *Acta Mater.* **51**, 4679–4691.

Burgers, W. (1934). *Physica*. **1**, 561–586.

Callahan, P. G., Simmons, J. P., & Graef, M. D. (2013). *Modell. Simul. Mater. Sci. Eng.* **21**, 015003.

Cho, J.-H., Rollett, A. D., & Oh, K. H. (2005). *Metall. Mater. Trans. A*. **36**, 3427–3438.

Davies, P. S., Wynne, B. P., Rainforth, W. M., Thomas, M. J., & Threadgill, P. L. (2011). *Metall. Mater. Trans. A*. **42**, 2278–2289.

Gey, N. & Humbert, M. (2003). *J. Mater. Sci.* **38**, 1289–1294.

Glavicic, M., Kobryn, P., Bieler, T., & Semiatin, S. (2003a). *Materials Science and Engineering: A*. **346**, 50–59.

Glavicic, M., Kobryn, P., Bieler, T., & Semiatin, S. (2003b). *Materials Science and Engineering: A*. **351**, 258–264.

Glavicic, M., Kobryn, P., & Semiatin, S. (2004). *Materials Science and Engineering: A*. **385**, 372–376.

Hefferan, C. M., Lind, J., Li, S. F., Lienert, U., Rollett, A. D., & Suter, R. M. (2012). *Acta Mater.* **60**, 4311–4318.

Humbert, M., Wagner, F., Moustahfid, H., & Esling, C. (1995). *J. Appl. Crystallogr.* **28**, 571–576.

Li, S. F., Lind, J., Hefferan, C. M., Pokharel, R., Lienert, U., Rollett, A. D., & Suter, R. M. (2012). *J. Appl. Crystallogr.* **45**, 1098–1108.

Li, S. F. & Suter, R. M. (2013). *J. Appl. Crystallogr.* **46**, 512–524.

Lienert, U., Li, S. F., Hefferan, C. M., Lind, J., Suter, R. M., Bernier, J. V., Barton, N. R., Brandes, M. C., Mills, M. J., Miller, M. P., et al. (2011). *JOM*. **63**, 70–77.

Lind, J., Li, S. F., Pokharel, R., Lienert, U., Rollett, A. D., & Suter, R. M. (2014). *Acta Mater.* **76**, 213–220.

Lutering, G. & Williams, J. (2003). Titanium Springer-Verlag, Berlin, Heidelberg.

Moustahfid, H., Gey, N., Humbert, M., & Philippe, M. J. (1997a). *Metall. Mater. Trans. A*. **28**, 51–61.

Moustahfid, H., Humbert, M., & Philippe, M. J. (1997b). *Acta Mater.* **45**, 3785–3790.

Pilchak, A. L. & Williams, J. C. (2011). *Metall. Mater. Trans. A*. **42**, 773–794.

Pokharel, R., Lind, J., Li, S. F., Kenesei, P., Lebensohn, R. A., Suter, R. M., & Rollett, A. D. (2015). *Int. J. Plast.* **67**, 217–234.

Sargent, G. A., Kinsel, K. T., Pilchak, A. L., Salem, A. A., & Semiatin, S. L. (2012). *Metall. Mater. Trans. A*. **43**, 3570–3585.

Stanford, N. & Bate, P. S. (2004). *Acta Mater.* **52**, 5215–5224.

Suter, R. M., Hennessy, D., Xiao, C., & Lienert, U. (2006). *Rev. Sci. Instrum.* **77**, 123905.

Tiley, J. S., Shiveley, A. R., Pilchak, A. L., Shade, P. A., & Groeber, M. A. (2014). *J. Microsc.* **255**, 71–77.

Wielewski, E., Menasche, D. B., Callahan, P. G., & Suter, R. (2015). URL: http://dx.doi.org/10.5525/gla.researchdata.163